Effect of oblique polymer pillars on spreading and elongation of rat mesenchymal stem cells

Jie Hu, Yan-Jun Liu, Jian Shi, Li Wang, Matthieu Piel, Yong Chen

Effect of oblique polymer pillars on spreading and elongation of rat mesenchymal stem cells

Jie Hu[1,2], Yan-Jun Liu [3], Jian Shi[1], Li Wang[1], Matthieu Piel[3] and Yong Chen[1*]

[1] *PASTEUR, Département de Chimie, École Normale Supérieure, PSL University, Sorbonne Université, CNRS, 75005 Paris, France*

[2] *Micro and Nano System Research Center, College of Information and Computer, Taiyuan University of Technology, Taiyuan, 030024, Shanxi, China*

[3] *Institut Curie, CNRS UMR 144, 26 rue d'Ulm, 75248 Paris Cedex 05, France*

* Corresponding author. Email: hujie@tyut.edu.cn;yong.chen@ens.fr

Abstract

Stiffness and anisotropy of culture substrates are important factors influencing the cell behavior and their responses to external stimuli. Herein, we report a fabrication method of oblique polymer pillars which allow modulating both stiffness and anisotropy of the substrate for spreading and elongation studies of Rat Mesenchymal Stem Cells (RMSCs). Poly (Lactic-co-Glycolic Acid) (PLGA) has been chosen to produce micro-pillars of different heights and different pitches using a combined method of soft-lithography and hot embossing. The stiffness of such pillar substrates varies over a large range so that RMSCs show effectively different spreading behaviors which are also sensitive to the inclining angle of the pillars. Our results showed that with the increase of the pillar height the area of cell spreading decreases but the cell elongation aspect ratio increases. Moreover, cells preferentially elongate along the direction perpendicular to that of the pillars' inclining, which is in agreement with the calculated anisotropy of the pillar substrate stiffness.

Keywords: Microfabrication, Oblique micropillars, Cell culture, Cell elongation

1. Introduction

Many in-vitro assays rely on cell culture, which is sensitive to both morphology and stiffness of the substrate, in addition to other micro-environmental factors such as surface biochemistry, shear force, etc. [1-3]. Typically, cells interact with the substrate by remolding the cytoskeletal and the intracellular signaling pathways, resulting in different behaviors, including cell adhesion [4-7], proliferation [8-10], migration [11-17], differentiation [18-20], apoptosis [21,22], aggregation [23] and tissue formation [24]. Consequently, it is important to be able to modulate the substrate morphology and stiffness for in-vitro assays as well as regenerative medicine [25-27].

In general, the interplay of cell-material systems is more efficient when the Young's modulus of the substrate is comparable to that of the cells. Due to the large variety of the cells or tissues, different types of substrates have to be considered. For example, gel layers are generally used to create low stiffness substrates [28]. By changing the polymer of ion concentration of the initial solution, the thickness of the gel layer and/or the processing parameters, the stiffness of the gel-layer coated substrate can be modulated. Alternatively, elastomer micropillars are used for more quantitative studies of cell-material interaction mechanisms [29]. Indeed, micropillars of different size, different height and different pitch size have been produced in polydimethylsiloxane (PDMS) by soft-lithography, and used for systematic investigations of cell mechanics [30]. On such substrates, high aspect ratio PDMS pillars can be deflected due to cellular forces [31-38]. However, it is not easy to produce high density PDMS pillars with both small size and high aspect ratio due to processing difficulties and pillars' collapse. To overcome this problem and to demonstrate the effect of directed migration, oblique PDMS pillars were used on the top of the cell layer cultured on a rigid substrate [11]. Finally, three-dimensional lattice-type PDMS structures were fabricated to demonstrate the substrate dependencies of pluripotent stem cell culture and neuronal growth [39].

In this work, we developed a fabrication method to produce high aspect ratio polymer pillars of smaller feature sizes with comparable stiffness of PDMS pillar and to demonstrate anisotropic elongation of cells on oblique pillar arrays. Hot embossing has been chosen to

produce pillars in Poly-lactic-co-glycolic acid (PLGA) for culture of Rat Mesenchymal Stem Cells (RMSCs). Hot embossing is a popular technique to manufacture surface structure of thermoplastic polymers polystyrene (PS), polymethylmethacrylate (PMMA), polycarbonate (PC), etc. Among them, PLGA has a relative low glass transition temperature so that it can be easily embossed. In addition, PLGA is biodegradable and widely used in biology and biomedical studies. The Young's modulus of PLGA is sufficient large to prohibit the pillars collapse. The stiffness of pillar substrate is a function of both material Young's modulus and pillars ratio. Despite its relative large Young's modulus, PLGA pillar substrates with small feature sizes but high aspect ratios should have compatible effective stiffness of PDMS pillars of relative large feature sizes. The fabrication method we developed is based on a bench process involving photolithography, soft-lithography and hot embossing. Our results showed that RMSCs could efficiently deflect the PLGA pillars so that their culture behaviors were clearly affected (Fig.1). In agreement with theoretical modeling, we observed that with the increase of the pillar height the cell spreading is less important but the spreading anisotropy is more pronounced.

2. Materials and methods

2.1 Chemicals and materials

The PLGA (poly(dl-lactide-co-glycolide) 85:15, Mw=50,000-75,000) was purchased from Sigma-Aldrich (France). The SU-8 photoresist and developer were obtained from MicroChem Corp (Newton, MA, USA). PDMS (Poly(dimethylsiloxane)) RTV 615 was purchased from GE Silicones (Waterford, NY, USA). The commercial blank plates coated with 1000 Å thick chrome and 1 μm thick AZ 1518 positive photoresist were obtained from CIPEC Company (Nanofilm, France). RMSCs were supplied by Etablissement Francais du Sang Centre-Atlantique (France). DMEM (Dulbecco's minimum essential medium), PBS tablets, Fetal bovine serum (FBS), Glutamine, Glutamine, Penicillin/Streptomycin (P/S), antibiotics (penicillin and streptomycin mix), Fungizone, bovine serum albumin (BSA), 0.05% Trypsin–EDTA solution, Triton-X-100 (TX), 4,6-diamidino-2-phenylindole (DAPI), Alexa Fluor TM 488 Phalloidin were obtained from Life Technologies. Trichloromethylsilane (TMCS), fibronectin (FN) and others chemicals of analytical grade were purchased from

Sigma-Aldrich (France).

2.2 Preparation of oblique micropillars

PLGA oblique micropillars were designed according to the theoretical estimation described as in discussion and produced by a combined method of conventional photolithography, soft lithography and hot embossing. The optical mask was first prepared using a micro pattern generator (μPG101, Heidelberg, Germany) and a blank Cr plate coated with 1μm thick of photoresist (Microchem). The master mold was obtained by backside exposure of a SU-8 photoresist layer spin-coated on the optical mask with a UV light at a given incident angle (Fig. 2a and b). After spin-coating and soft baking on hot plate at 65℃ for 1 min and 95℃ for 2 min, the exposure of the SU8 photoresist layer was performed with a UV light of 365 nm wavelength and power density of 160 mJ/cm^2 for 8 s. Then, the photoresist layer was post-baked at 65 ℃ for 1 min and 95 ℃ for 2 min on hot plate. After development and rinsing with isopropyl alcohol, the oblique micropillar arrays of SU8 were obtained as the master mold pattern. The master mold was then treated using TMCS vapor and then casted with mixture of PDMS pre-polymer (RTV 615) at a 1:5 ratio. After curing in an oven at 80 ℃ for 4 hours, the PDMS casting layer was gently released from the master and treated by TMCS evaporation. Finally, the obtained PDMS layer was used as hot embossing mold to replicate the micro pillar patterns into a PLGA layer (a, c).

Fig. 2b shows the homemade tilting stage under vertical UV light with an inclination angle. In order to obtain the PLGA oblique micropillar pattern, hot embossing was performed on PDMS mold and PLGA substrate, as shown in Fig. 2c. Firstly, the PLGA film (3 mm in thickness) was prepared by compression molding. Secondly, the PLGA film was placed on glass slide and covered with the PDMS mold. Subsequently, this assembly was placed between two hot plates of a hydraulic press (Specac, UK). Then, the temperature of the hot plates was raised to 90℃, which is well above the glass transition temperature (T_g) of PLGA (45-50℃). Allowing about 2 min for the PLGA film to melt, the PDMS mold was embossed into the PLGA film by applying a constant pressure120 kPa for 5 min. After cooling down to room temperature, the pressure was released and PDMS mold was removed, the desired PLGA oblique micropillars pattern (size: 1cm×1cm) can be obtained on the surface of glass

slide, as shown in Fig. 2d. Meanwhile, the vertical micropillar arrays were also fabricated combing photolithography with hot embossing method for cell culture in control experiment, as shown in Fig. 2e.

2.3 RMSCs cell culture

RMSCs were cultured in DMEM medium supplemented with 20% fetal bovine serum (FBS), 1% Glutamine, 1% antibiotics and 0.01% Fungizone at 37℃ in a humidified atmosphere containing 5% CO_2. Before seeding, the as-prepared oblique micropillar arrays was exposed to ultraviolet light for 30 min and placed in 60-mm petri dish for cell culture. Then, cells were dissociated with 0.05% Trypsin-EDTA solution at 37℃ for 3 min and resuspended in the medium after centrifugation. The PLGA oblique micropillar arrays were washed by immersing in 98% ethanol for 30 min and sterilized using mild cell-culture grade UV light for 30 min, and then incubated in 50 μg/ml fibronectin in DPBS at room temperature for 30 min. After rinsing three times with sterilized 1x PBS, cells were seeded on the oblique micropillar pattern surface at a density of 1×10^4 cells/cm^2 and cultured for 48 h for cell adhesion and spreading.

2.4 Immunofluorescent imaging

Before observation, RMSCs were first fixed in 1x PBS containing 4% formaldehyde for 30 min. Then, the sample was washed with PBS three times and cells were permeabilized with PBS containing 0.5% Triton- X-100 (TX) for 10 min and washed again with PBS three times. Afterward, cells were blocked in antibody diluting solution (AbDil, PBS containing 0.1% TX, 3% BSA, 0.1% Azide (V:V)) at room temperature for 30 min and washed with PBS for three times. Cytoskeleton and nucleus of the cells were stained by Phalloidin-FITC and DAPI at the same time for 20 min and washed again with PBS for three times before imaging. Optical images were recorded using a fluorescence microscope (Zeiss, Axiovert 200, Germany) equipped with a B&W CCD camera (Evolution QEi, Canada).

2.5 Scanning electronic microscopy (SEM)

High-resolution images of the sample were obtained with a scanning electron microscope (SEM, Hitachi S-800) operated at 10 kV. Cells were fixed in PBS containing 4% formaldehyde for 30 min, and then rinsed twice with PBS and stabilized by immersion in 30%

ethanol (in DI) for 30 min. Afterward, cells were dehydrated in a graded series of ethanol: 50%, 70%, 80%, 90% and 100% every 10 min for two times, followed by nitrogen gas drying. Finally, the samples were deposited a thin film of gold of 10 nm thickness by a sputter (Auto500, UK) for SEM observation.

2.6 Image analysis

The Image J software (open source image analysis software) was introduced to analyze the fluorescence images of cells. Cell cytoskeleton was highlighted by adjusting threshold of the brightness, outlined, and best-fitted with ellipses. From the ellipses, the cell cytoskeleton area, major and minor axes, and angle between the major axis and the reference direction were then computed. The alignment angles and elongation aspect ratio were calculated accordingly.

2.7 Statistical analysis

All errors indicated in the text are s.e.m. Non parametric, two tailed, Mann-Whitney t test was performed to determine whether the difference between two groups was significantly different in their mean value (using GraphPad Prism 5). **$p < 0.01$ and ***$p < 0.001$ according to t test.

3. Results and discussion

3.1 Fabrication performance of PLGA oblique micropillars

PLGA is a biocompatible and biodegradable copolymer widely used for biomedical applications. It has also been approved for clinical use in humans by the U.S. Food and Drug Administration (FDA). The reason of using a PDMS mold to replicate oblique PLGA micropillars is that it is relatively easy due to the low Young's modulus of PDMS. To decrease the risk of the PDMS deformation, a hard PDMS at ratio 5:1 was chosen. Our embossing results showed that high density and high aspect ratio PLGA pillars could effectively replicated by hot-embossing despite the low Young's modulus of PDMS. The reason of using a two-step casting process is that it is relatively easy to fabricate high resolution and high aspect ratio of SU8 pillars and replicate them by PDMS casting. Finally, the backside exposure of the SU-8 resist was used to minimize the diffraction effect due to intimate contact between the resist and the master pattern. As a result, we produced

micropillar arrays with the same diameter of 1.5 μm but different height (H) ranging from 2 to 10 μm and different pitches (S) ranging from 4 to 10 μm. For clarity, the samples were labeled as H_mS_n, where m, n respectively represents the height and the pitch of the pillars. Fig. 3 shows SEM micrographs of the PLGA oblique micropillars. Comparing to PDMS, PLGA has a much larger Young's modulus but pillars of smaller diameters and/or larger height can still be used for cell force measurements.

3.2 Effect of cell elongation

When RMSCs were placed on the PLGA pillar substrate, they adhered after 48 h and then spread accordingly. As illustrated by the single cell SEM images of Fig. 1d and f, the cell on a vertical pillar array showed no preferential orientation but that on an oblique pillar array was elongated along the direction perpendicular to the pillars inclining. The higher magnitude SEM images showed the different pillar deflection on the left (Fig. 1e) and the right (Fig. 1g) edge of the cell spreading area. Moreover, the effective stiffness of the oblique pillar substrate is anisotropic and the cell spread more easily in the direction perpendicular to the pillars inclining. This can be explained based on a simple stiffness model.

According to the Euler-Bernoulli beam theory, the spring constant of an elastic pillar can be calculated by $K = 3\pi ED^4/64H^3$, which defines the ratio of applied force (F) and the distance of deflection on the top of the pillar (δ), i.e. $K = F/\delta$, where D is the diameter of pillar, H *is* the height, E is the Young's modulus of PLGA (~1GPa) [40]. The equivalent Young's modulus (E_p) of a dense pillar array can be calculated by $Ep = 9\mathrm{K}/2\pi\mathrm{D}$ [31]. In our case, the diameter of the PLGA pillars is 1.5 μm and the height varies in the range between 2 and 10 μm, corresponding to an equivalent Young's modulus varying from 88.98 MPa (H = 2 μm) to 0.712 MPa (H = 10 μm). For oblique pillars with small inclining angles, we define a factor ε to take into account the stiffness anisotropy of the substrate such that $\delta = \varepsilon F/K$, where $\varepsilon = sin^2\varphi + cos^2\varphi \sin^2\vartheta$, with ϑ and φ respectively the angle between the pillar and the substrate and the angle between the direction of traction force and the projected orientation of the pillar in the plane. As a result, numeric calculation showed an increased angle dependence of ε or the anisotropy of the effective stiffness of the substrate with decrease of ϑ (Fig. 1c), which explains the elongation of the cells along the direction

perpendicular to the oblique pillar's orientation.

3.3 Morphological analyses of cell on oblique micropillars

The elongation of RMSCs on oblique PLGA pillars could be systematically observed. For comparison, Fig. 1h and i display the immunofluorescence images of RMSCs on the border areas of vertical micropillars (H_5S_4) and oblique pillar arrays (H_5S_4) after 48 h incubation. On the left and right areas of the two images separated by the dashed lines are cells on flat and pillar areas, respectively. The inclining direction of the pillars is indicated by a white arrow. Clearly, RMSCs on flat PLGA areas as well as on vertical pillars showed no preferential orientation, except those on the border. While, when cell were cultured on flat PLGA surface and PLGA oblique micropillars, RMSCs on oblique pillars were strongly elongated in the direction perpendicular to the inclining.

To further investigate the influence of cell behaviors on oblique micropillars pattern, RMSC have been cultured on PLGA oblique micropillar arrays with different heights (2, 5 and 10 μm) and different pitches (4, 6, 8 and 10 μm). After 48h culture, cell nuclei were stained by DAPI (blue) and F-actin by Alexa Fluor TM 488 phalloidin (green). Fig. 4 a-d shows immunofluorescent images of RMSC cells on PLGA oblique micropillars with 2 μm height and pitches 4, 6, 8 and 10 μm. The obtained results exhibit that cells are more spread on 2 μm height pillars, showing ruffled lamellipodia and almost the same spreading area as on a flat surface. These data suggest that the small height pillars of PLGA have no strong effect on cell spreading. Indeed, these short pillars are too small to be deflected by contractile forces of the cells and thus cells experience no difference between such pillars arrays and a flat surface. Additionally, cells on such short micropillars may also attach as adhere to the flat surface at the bottom of the pillars, exploring the full space for spreading.

For oblique micropillars with height of 5 μm, it seems that cell spreading is rapidly decrease, which is likely due to the decrease of the effective stiffness of the substrate. On H_5S_4 pillars (Fig. 4e), a high degree of cell spreading anisotropy was observed, with cells elongating in the direction perpendicular to the pillar inclining. Indeed, cells spread on such a dense pillar array without touching the floor and their spreading behavior was solely determined by the pillars. Conversely, on H_5S_6; H_5S_8 and H_5S_{10} pillar arrays (Fig. 4f-h), the

pitch and the spacing of the pillars are larger than or comparable to the height. As a consequence, cells were able to adhere to the flat floor between the pillars and did not display any clear elongation anisotropy.

On 10 μm height oblique micropillars, the height is larger than or comparable to the pitch. As a consequence, cell spreading could also be guided by single lines of micropillars, depending on the distance between micropillars. On $H_{10}S_4$ micropillars (Fig. 4i), cells had a biased elongation along the direction perpendicular to the pillar inclining, while on $H_{10}S_6$ pillars (Fig. 4j), the distance between the pillars might dominate, as cells were found to be elongated along single lines of micropillars either parallel or perpendicular to the pillar inclining direction. On $H_{10}S_8$ and $H_{10}S_{10}$ micropillars (Fig. 4k and l), this effect was lost likely because cells could reach the flat floor between the pillars.

3.4 Statistical data

The extent of the bias in cell spreading on different substrates can be statistically analyzed by measuring the surface area and the orientation of stained actin fibers for each cell. The actin cytoskeleton was highlighted by adjusting threshold of the brightness, and best-fitted with ellipses. From the ellipses, the actin cytoskeleton surface area, major and minor axes, and angle between the major axis and the reference direction were then computed. All cells in contact with other cells or at the edge of the image were manually removed from the data sets. Elongation is characterized by the ratio between the length of the major axis (*l*) and that of the minor axis (w) of the ellipse, while alignment is defined by the angle between the major axis of the ellipse and the direction perpendicular to that of pillars inclining. In polar plots of Fig. 5, the alignment angle and the elongation aspect ratio of RMSCs on different pillar arrays are displayed. The actin fibers of the cells on H_2 pillars extended in all directions with an elongation aspect ratio in the range of 1.5~3.5, which is slightly larger than that on flat PLGA surfaces. On H_5 and H_{10} pillars, an oriented elongation effect was remarkably presented but the effect decreases with the increase of the pillar pitch. The actin cytoskeleton and nuclei areas of individual RMSCs on different pillar arrays are compared in Fig. 6. On H_2 pillars, the average cell area was about 17160 ± 120 μm^2, which was significantly larger than that on H_5 (9809 ± 114 μm^2) and H_{10} (3503 ± 56 μm^2) pillars.

Without changing the pillar pitch, the average cell area decreases remarkably with the increase of the pillar height, indicating that the average cell area was mostly determined by the height of pillar. Without changing the pillar height, the average cell area on H_2 pillars is significantly larger than that of H_5 and H_{10}, suggesting that cells may follow on the floor of PLGA structures. Interestingly, the nuclear area of the cell on pillars was correlated to the cell spreading area, likely due to the internal constrains exerted on the nucleus by the cytoskeleton.

4. Conclusions

We fabricated PLGA oblique micropillars with different heights and different pitches by a combined use of inclined UV lithography, soft lithography and hot embossing techniques. The effective stiffness of the designed pillar arrays was calculated, showing strong anisotropy in the range of 88.98 MPa (H = 2 μm) and 0.712 MPa (H = 10 μm) for PLGA micropillars. In agreement with the theoretic calculation, our experimental data have shown strong effects of the oblique micropillars on cell spreading and elongation. To some extent, cells have been shown to exhibit contact guidance when cultured on anisotropic substrate. We found that in the case of RMSCs the average spread area of the cells decreased but their elongation aspect ratio increased with the increase of the pillar height. Surprisingly, the cells elongated along the axis perpendicular to that of pillars' inclining due to the regulation of the intracellular forces. Finally, the current method should be able to pattern other bio-compatible polymers or nanoscale features as previously reported [41].

Acknowledgments

This work was supported by Agence de Recherche Nationale under contract ANR-17-CE09-0017 (AlveolusMimics), European Commission Cost Action BIONECA (CA 16122), DIM ELICIT program of Ile-de-France, and PSL Valorization through Pre-maturation project.

References

[1] Discher D E, Janmey P, Wang Y, 2005. Tissue cells feel and respond to the stiffness of their substrate. Science. 310(5751): 1139-1143.

[2] Madl C M, Heilshorn S C, Blau H M, 2018. Bioengineering strategies to accelerate stem cell

therapeutics. Nature. 557(7705): 335.

[3] Darnell, Max, Luo Gu, and David Mooney, 2018. RNA-seq reveals diverse effects of substrate stiffness on mesenchymal stem cells. Biomaterials. 181, 182-188.

[4] Wang B, Tu X, Wei J, Wang L and Chen Y, 2018. Substrate elasticity dependent colony formation and cardiac differentiation of human induced pluripotent stem cells. Biofabrication. 11 015005.

[5] Wang B, Wei J, Tu X, Shi J, and Chen Y, 2019. Fabrication of elastomer pillar arrays with elasticity gradient for cells migration, elongation and patterning, Biofabrication 11, 045003

[6] Jiyun Jeong,Yeolin Lee, Yeongeun Yoo, Myung Kyu Lee, 2018. Specific capture, recovery and culture of cancer cells using oriented antibody-modified polystyrene chips coated with agarose film. Colloids and Surfaces B: Biointerfaces.162, 306-315.

[7] GuicaiLi, ShiyuChen, MingZeng, YanKong, FeiZhao, Luzhong Zhang and YuminYang, 2019. Hierarchically aligned gradient collagen micropatterns for rapidly screening Schwann cells behavior. Colloids and Surfaces B: Biointerfaces.176, 341-351.

[8] Bourkoula, A., Constantoudis, V., Kontziampasis, D., Petrou, P. S., Kakabakos, S. E., Tserepi, A., and Gogolides, E. (2016). Roughness threshold for cell attachment and proliferation on plasma micro-nanotextured polymeric surfaces: the case of primary human skin fibroblasts and mouse immortalized 3T3 fibroblasts. Journal of Physics D: Applied Physics, 49(30), 304002.

[9] IvanDing, Jenna A.Walz, Charles R.Mace and Amy M.Peterson, 2019. Early hMSC morphology and proliferation on model polyelectrolyte multilayers. Colloids and Surfaces B: Biointerfaces. 178, 276-284.

[10] Sisi Li, Francesco Paolo Ulloa Severino, Jelena Ban, Li Wang, Giulietta Pinato, Vincent Torre and Yong Chen, 2018. Improved neuron culture using scaffolds made of three-dimensional PDMS micro-lattices. Biomedical Materials. 13, 034105.

[11] Le Berre M, Liu Y J, Hu J, Maiuri P, Bénichou O, Voituriez R, Chen Y and Piel M, 2013. Geometric friction directs cell migration. Physical review letters. 111, 198101.

[12] Hua Zhang, Ruixia Hou, Peng Xiao, Rubo Xing, Tao Chen, Yanchun Han, Penggang Ren and Jun Fu, 2016. Single cell migration dynamics mediated by geometric confinement. Colloids and Surfaces B: Biointerfaces. 145, 72-78.

[13] Liang E I, Mah E J, Yee A F and Digman M A, 2017. Correlation of focal adhesion assembly and disassembly with cell migration on nanotopography. Integrative Biology. 9, 145.

[14] Han L, Mao Z, Wu J, Guo Y, Ren T and Gao C, 2013. Unidirectional migration of single smooth

muscle cells under the synergetic effects of gradient swelling cue and parallel groove patterns. Colloids and Surfaces B: Biointerfaces. 1111, 6.

[15] Kojima T, Moraes C, Cavnar S P, Luker G D and Takayama S, 2015. Surface-templated hydrogel patterns prompt matrix-dependent migration of breast cancer cells towards chemokine-secreting cells. Acta biomaterialia. 13, 68.

[16] Yanez-Soto B, Liliensiek S J, Gasiorowski J Z, Murphy C J and Nealey P F, 2016. The influence of substrate topography on the migration of corneal epithelial wound borders. Biomaterials. 34, 9244.

[17] Ko Y G, Co C C and Ho C C, 2013. Directing cell migration in continuous microchannels by topographical amplification of natural directional persistence. Biomaterials. 34, 353.

[18] Zhang S, Ma B, Li, F, Duan J, Wang S, Qiu J and Liu H, 2018. Polylactic Acid Nanopillar Array-Driven Osteogenic Differentiation of Human Adipose-Derived Stem Cells Determined by Pillar Diameter. Nano letters. 18, 2243.

[19] Seo H R, Joo H J, Kim D H, Cui L H, Choi S C, Kim J H and Lim D S, 2017. Nanopillar Surface Topology Promotes Cardiomyocyte Differentiation through Cofilin-Mediated Cytoskeleton Rearrangement. ACS applied materials & interfaces. 9, 16803.

[20] Kyle D J, Oikonomou A, Hill E and Bayat A, 2015. Development and functional evaluation of biomimetic silicone surfaces with hierarchical micro/nano-topographical features demonstrates favourable in vitro foreign body response of breast-derived fibroblasts. Biomaterials. 52, 88.

[21] Jeon H, Tsui J H, Jang S I, Lee J H, Park S, Mun K and Kim D H, 2015. Combined effects of substrate topography and stiffness on endothelial cytokine and chemokine secretion. ACS applied materials & interfaces. 7, 4525.

[22] Vini Gautam, Shagufta Naureen, Naeem Shahid, Qian Gao, Yi Wang, David Nisbet, Chennupati Jagadish and Vincent R Daria, 2017. Engineering highly interconnected neuronal networks on nanowire scaffolds. Nano letters. 17, 3369.

[23] Glass D S and Riedel-Kruse I H, 2018. A synthetic bacterial cell-cell adhesion toolbox for programming multicellular morphologies and patterns. Cell.174(3): 649-658

[24]Yi Wang, Wenguo Cui, Joshua Chou, Shizhu Wen, Yulong Sun and Hongyu Zhang, 2018. Electrospun nanosilicates-based organic/inorganic nanofibers for potential bone tissue engineering. Colloids and Surfaces B: Biointerfaces, 172, 90-97.

[25] Xiaoli Xu, Lunkun Ma, Yanjiao Wu and Liling Tang, 2018. Micropillar-based culture platform

induces epithelial-mesenchymal transition in the alveolar epithelial cell line. Journal of Biomedical Materials Research Part A. 106, 3165.

[26] Caprettini V, Cerea A, Melle G, Lovato L, Capozza R, Huang J A and De Angelis F, 2017. Soft electroporation for delivering molecules into tightly adherent mammalian cells through 3D hollow nanoelectrodes. Scientific reports. 7, 8524.

[27] Rashidi H, Yang J and Shakesheff K M, 2014. Surface engineering of synthetic polymer materials for tissue engineering and regenerative medicine applications. Biomaterials Science. 2,1318.

[28] Wanqu Zhu, Byoung Choul Kim, Mingyi Wang, Jessie Huang, Abraham Isak, Natalia M. Bexiga, Robert Monticone, Taekjip Ha, Edward G. Lakatta and Steven S. An, 2018. TGFβ1 reinforces arterial aging in the vascular smooth muscle cell through a long-range regulation of the cytoskeletal stiffness. Scientific reports. 8(1), 2668.

[29] Seyedeh Atefeh Mobasseri,Sebastiaan Zijl,Vasiliki Salameti,Gernot Walko,Andrew Stannard,Sergi Garcia-Manyes and Fiona M.Watt, 2019. Patterning of human epidermal stem cells on undulating elastomer substrates reflects differences in cell stiffness. Acta biomaterialia, 87, 256-264.

[30] Bin Wang, Li Wang, Yadong Tang, Jian Shi, Jin Wei, Xiaolong Tu, Yong Chen, 2018. Fabrication of spaced monolayers of electrospun nanofibers for three-dimensional cell infiltration and proliferation. Microelectronic Engineering. 198, 73-77.

[31] Fu J, Wang Y K, Yang M T, Desai R A, Yu X, Liu Z and Chen C S, 2010. Mechanical regulation of cell function with geometrically modulated elastomeric substrates. Nature methods. 7, 733.

[32] Yang M T, Fu J, Wang Y K, Desai R A and Chen C S, 2011. Assaying stem cell mechanobiology on microfabricated elastomeric substrates with geometrically modulated rigidity. Nature protocols. 6, 187.

[33] Théry M, 2010. Micropatterning as a tool to decipher cell morphogenesis and functions. Journal of cell science. 123, 4201.

[34] Ravasio A, Vaishnavi S, Ladoux B and Viasnoff V, 2015. High-resolution imaging of cellular processes across textured surfaces using an indexed-matched elastomer. Acta biomaterialia. 14, 53.

[35] Gao Y, Zhou B, Wu X, Gao X, Zeng X, Xie J, Wang C, Ye Z R, Wan J and Wen W J, 2015. Three Dimensional and Homogenous Single Cell Cyclic Stretch within a Magnetic Micropillar Array (mMPA) for a Cell Proliferation Study. ACS Biomaterials Science & Engineering. 2, 65.

[36] Sun Y, Yong A M A, Villa-Diaz LG, Zhang X, Chen W, Philson R, Weng S, Xu H, Krebsbach P H and Fu J, 2014. Hippo/YAP-mediated rigidity-dependent motor neuron differentiation of human

pluripotent stem cells. Nature Materials. 13, 599.

[37] Matschegewski C, Staehlke S, Loeffler R, Lange R, Chai F, Kern D P and Nebe B J, 2010. Cell architecture-cell function dependencies on titanium arrays with regular geometry. Biomaterials. 31, 5729.

[38] Schoen I, Hu W, Klotzsch E and Vogel V, 2010. Probing cellular traction forces by micropillar arrays: contribution of substrate warping to pillar deflection. Nano letters. 10, 1823.

[39] J. Li, F. Zhang, L. Yu, N. Fujimoto, M. Yoshioka, X. Li, J. Shi, H. Kotera, L. Liu and Y. Chen, 2017. Culture substrates made of elastomeric micro-tripod arrays for long-term expansion of human pluripotent stem cells. Journal of Materials Chemistry B. 5(2), 236-244.

[40] Park J H, Allen M G, Prausnitz M R. 2005. Biodegradable polymer microneedles: fabrication, mechanics and transdermal drug delivery. Journal of controlled release. 104(1): 51-66.

[41] Studer V, Pepin A, Chen Y. 2002. Nanoembossing of thermoplastic polymers for microfluidic applications. Applied physics letters.80(19): 3614-3616.

Figure captions:

Figure 1 Cells on vertical and oblique micropillar arrays: (a, b) Schematic of vertical (a) and oblique (b)

pillar arrays; (c) Polar plots of calculated anisotropy factor ε for different degree of pillar inclining; (d-g) SEM images of RMSC on vertical (d) and oblique (e-g) pillars, showing different behaviors of cell caused pillar defection. (h, i) Immunofluorescent images of RMSCs on the edge area of a vertical (h:H_5S_4) and oblique (i:H_5S_4) pillar arrays. The patterned and non-patterned area are separated by dashed line; F-actin was stained by Alexa Fluor 488 phalloidin (green); The white arrows indicate the the pillar inclining direction.

Figure 2 Fabrication of the PLGA oblique micropillars. (a) Process steps of the fabrication. (b) Backside exposure of the SU8 resist layer with a UV light at oblique incidence. (c) Schematic of hot embossing. (d) SEM images of the oblique (d) and vertical (e) PLGA micropillars.

Figure 3 SEM photographs of PLGA oblique micropillars with different heights (H) and different pitches (S) obtained by hot embossing using PDMS mold, where the subscript of H and S denotes the height and pitch in μm, respectively.

Figure 4 Immunofluorescent images of RMSCs on oblique PLGA micropillars, where the subscript of H and S denotes the height and pitch in μm, respectively. Cell nuclei were stained by DAPI (blue) and F-actin by Alexa Fluor 488 phalloidin (green). White arrows indicate the axis perpendicular to the pillar inclining direction.

Figure 5 Polar plots of cytoskeleton alignment (angular coordinate) and elongation (radial coordinate) of RMSCs grown on oblique pillars, where the subscript of H and S denotes the height and pitch in μm, respectively (Each data point represents a cytoskeleton of cell).

Figure 6 Distribution of cell skeleton (a) and nuclei area (b) spreading on oblique pillars of different heights and pitches (n=250 for each pillar surface). ** $p < 0.01$, *** $p < 0.001$ according to t test.

Figure 1

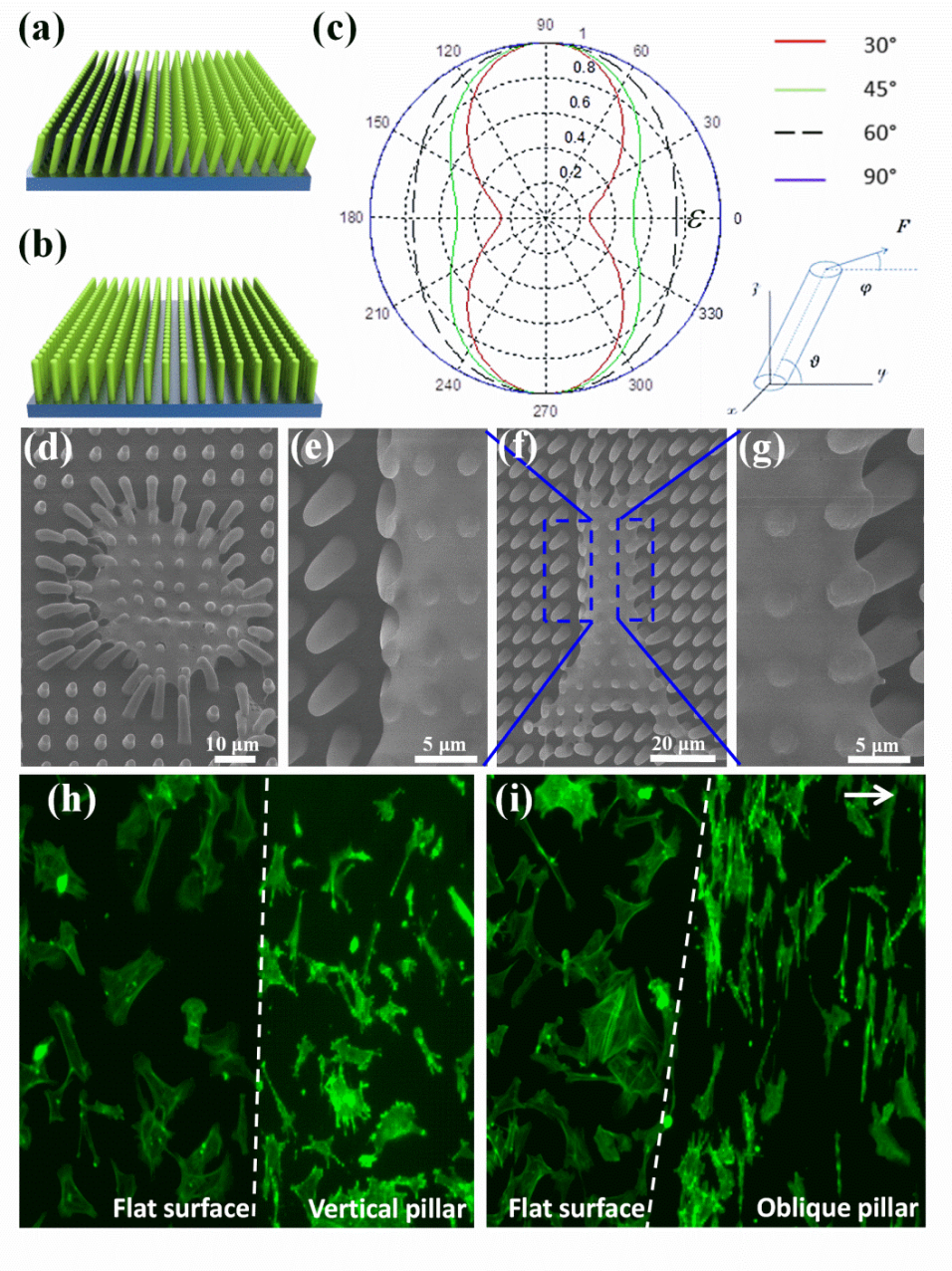
(a)
(b)
(c)
90
120
60
150
30
180
0
210
330
240
300
270
1
0.8
0.6
0.4
0.2
30°
45°
60°
90°
F
φ
ϑ
(d)
10 μm
(e)
5 μm
(f)
20 μm
(g)
5 μm
(h)
Flat surface
Vertical pillar
(i)
Flat surface
Oblique pillar

Figure 2

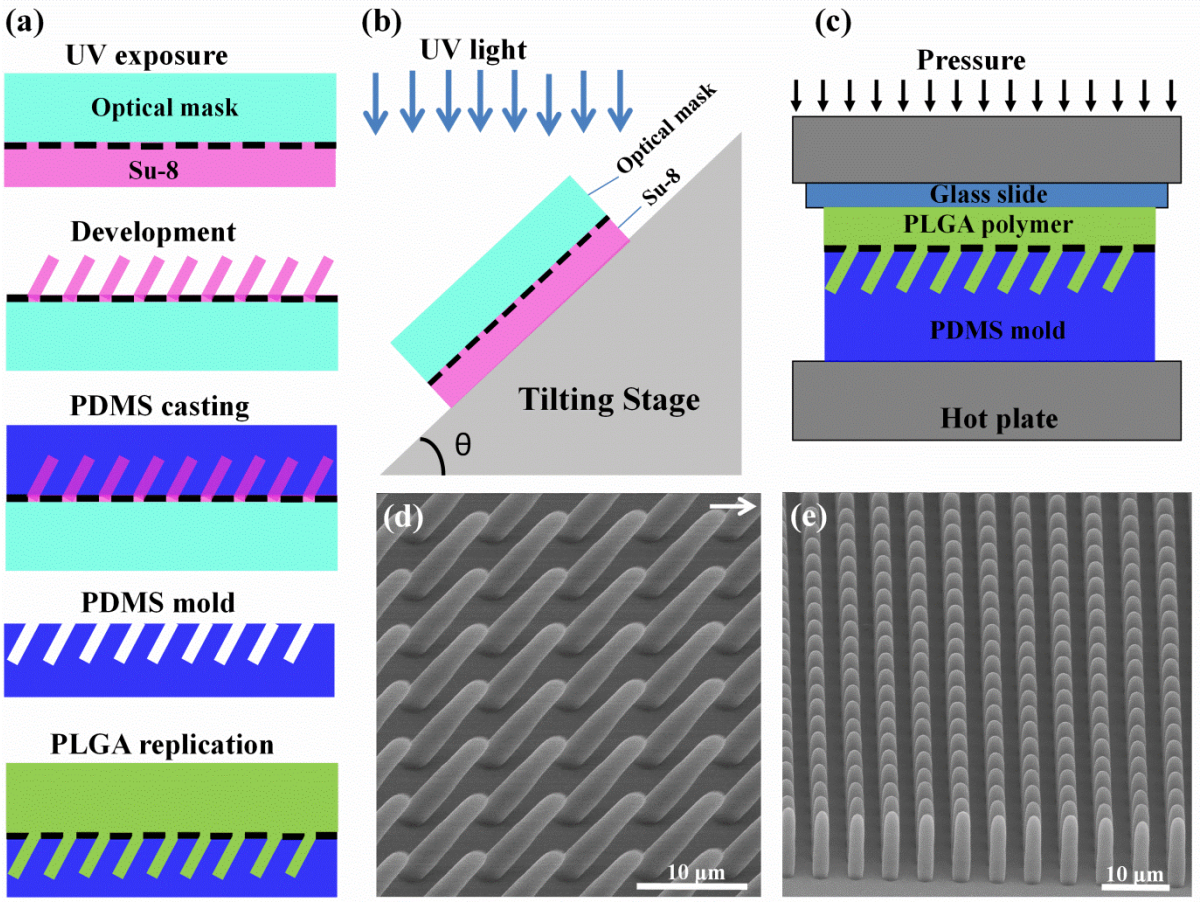
(a)
UV exposure
Optical mask
Su-8
Development
PDMS casting
PDMS mold
PLGA replication
(b)
UV light
Optical mask
Su-8
Tilting Stage
θ
(c)
Pressure
Glass slide
PLGA polymer
PDMS mold
Hot plate
(d)
10 μm
(e)
10 μm

Figure 3

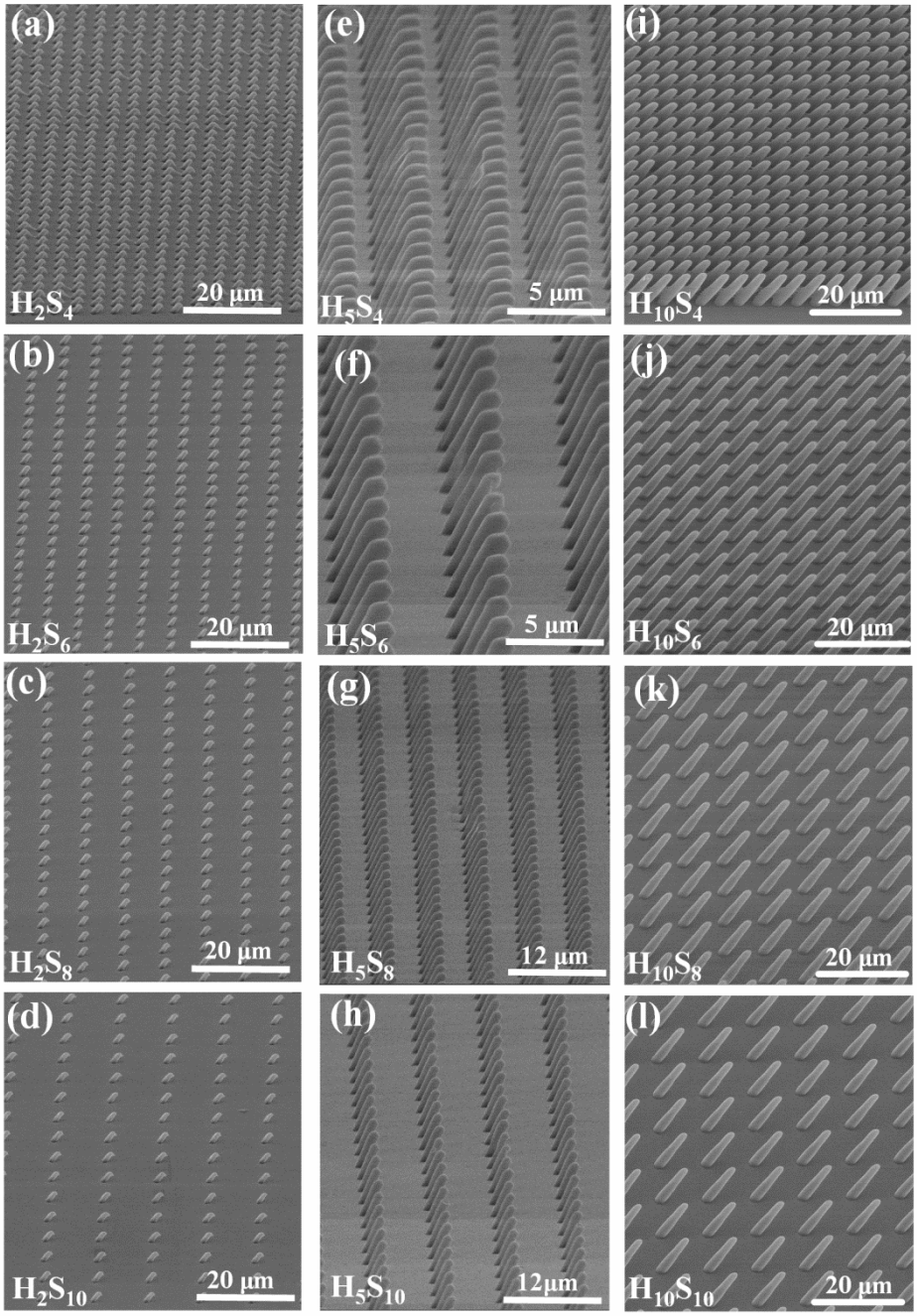
(a)
H2S4
20 µm
(e)
H5S4
5 µm
(i)
H10S4
20 µm
(b)
H2S6
20 µm
(f)
H5S6
5 µm
(j)
H10S6
20 µm
(c)
H2S8
20 µm
(g)
H5S8
12 µm
(k)
H10S8
20 µm
(d)
H2S10
20 µm
(h)
H5S10
12µm
(l)
H10S10
20 µm

Figure 4

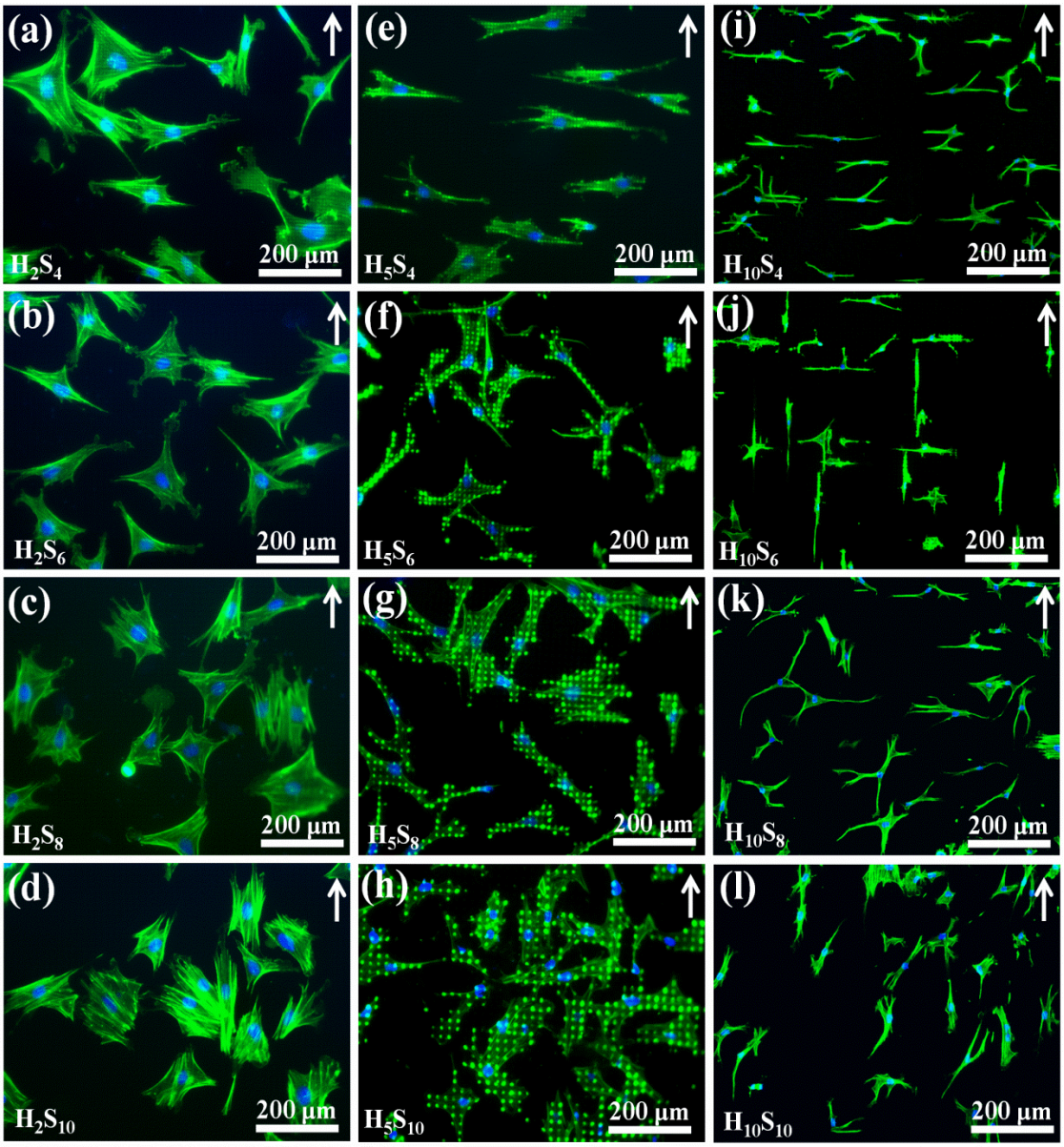
(a)
H2S4
200 µm
(e)
H5S4
200 µm
(i)
H10S4
200 µm
(b)
H2S6
200 µm
(f)
H5S6
200 µm
(j)
H10S6
200 µm
(c)
H2S8
200 µm
(g)
H5S8
200 µm
(k)
H10S8
200 µm
(d)
H2S10
200 µm
(h)
H5S10
200 µm
(l)
H10S10
200 µm

Figure 5

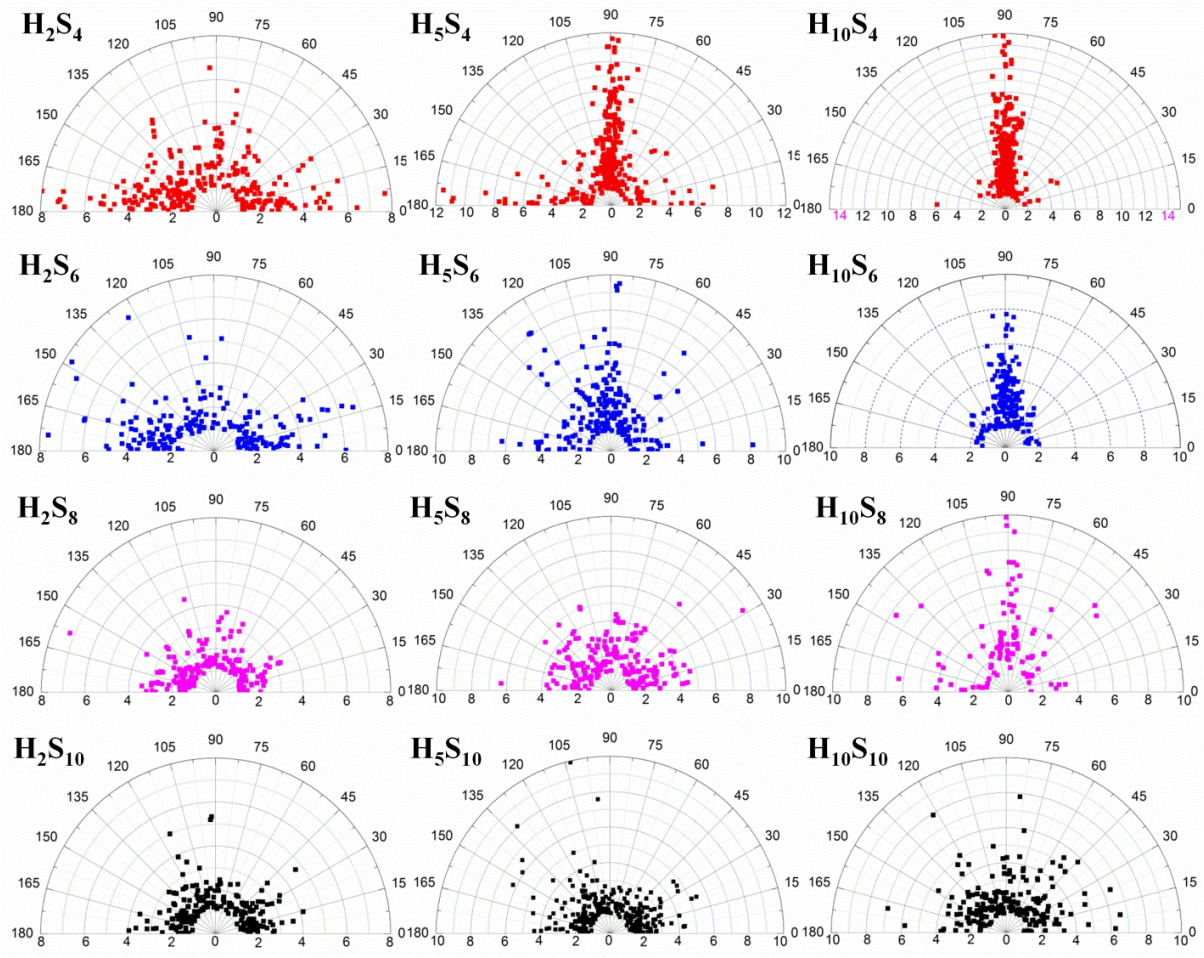
H2S4
H5S4
H10S4
H2S6
H5S6
H10S6
H2S8
H5S8
H10S8
H2S10
H5S10
H10S10

Figure 6

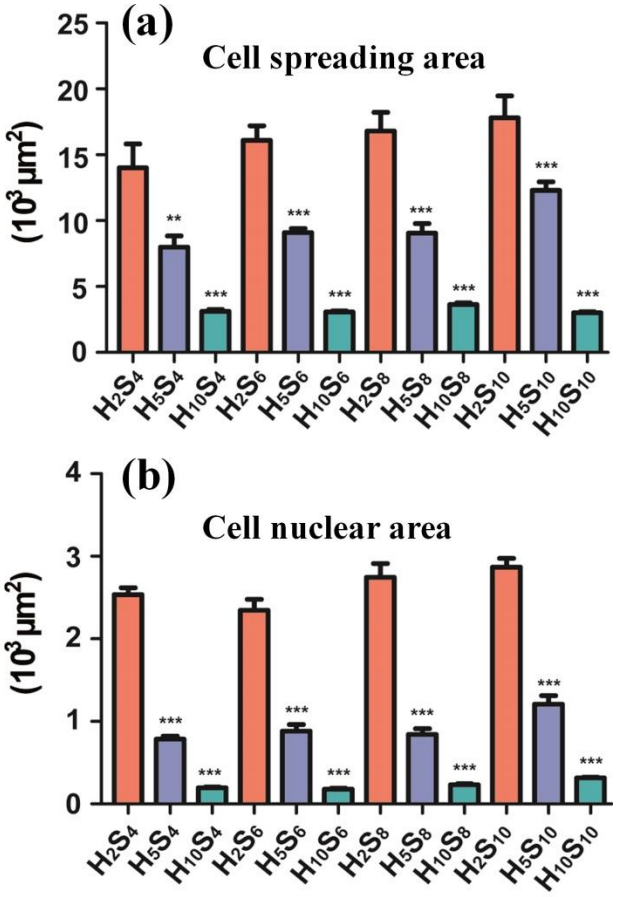
(a)
Cell spreading area
(10³ μm²)
25
20
15
10
5
0
**
***
H2S4
H5S4
H10S4
H2S6
H5S6
H10S6
H2S8
H5S8
H10S8
H2S10
H5S10
H10S10
(b)
Cell nuclear area
(10³ μm²)
4
3
2
1
0